Journal Name

ARTICLE

Na-ion diffusion in NASICON-type solid electrolyte: a density functional study

Received 00th January 20xx,

Accepted 00th January 20xx

DOI: 10.1039/x0xx00000x

www.rsc.org/

Kieu My Bui,[a,b,c] Van An Dinh,[d,e*] Susumu Okada,[b] and Takahisa Ohno[c,f,g*]

Based on the density functional theory, we have systematically studied the crystal and electronic structures, and diffusion mechanism of the NASICON-type solid electrolytes $Na_3Zr_2Si_2PO_{12}$. Four possible elementary processes are addressed: three inner-chain and one inter-chain processes. In inner-chain processes, Na tends to move inside the Na diffusion chain, while Na moves across the Na diffusion chain in inter-chain process. The activation energies for the inner-chain and inter-chain processes are 230 meV and 260 meV, respectively. By combining possible elementary processes, three preferable pathways along *a*, *b*, and *c* direction are found.

1. Introduction

Extensive research efforts have been made to meet the continuous raising of energy requirement of the modern world. Among many criteria for the future energy sources, two most important criteria are needed: performance and price. The batteries in portable devices are required to be more compact and efficient. Hence, there is a huge demand for the high energy density and high voltage sources. Moreover, the low cost criterion is also a must to stimulate the daily use appliances and mass production. On the battle of performance, Li-ion batteries (LIBs) are now playing the leading role with high gravimetric energy density (110-160 Wh/kg) and high voltage (3.6V).[1,2] A great deal of attention has been paid in both experimental and theoretical study of LIBs.[3–6] Nevertheless, in the battle of price, LIBs seem not to be a strong competitor because of the high price of Li and the lack of Li sources. Indeed, the abundance of Li in the Earth's crust is as small as 20ppm[7] and the Li source is unevenly distributed (mainly in South America). Hence, the search for a cheap material having comparable performance to LIBs is becoming an important issue. Standing next to Li in the first group of periodic table, Na is the second-lightest and smallest alkali metal after Li. Na-ion batteries (SIBs) are now attracting attention because of the lower price and higher abundance.[8–11] Na is not only the sixth richest abundance element on earth crust but also a widely distributed material. On the aspect of the material abundance and low cost, SIBs have potential to replace LIBs on large scale grid energy storage.

In SIBs, a problem that needed to be solved is the flammable liquid electrolytes because Na has high reactivity to moisture and oxygen causing high risk of unsafe operation. Hence, all-solid state batteries using non-flammable solid electrolytes have become trendy in designing energy storage devices.[12,13] The benefits of using all-solid state batteries are avoiding: electrolyte leakage, liquid electrolytes vaporization, and phase transition at low temperature. Also, the reliability of the all-solid state batteries is high since they have excellent storage stability and long cycle life. In addition, all-solid state batteries may prolong battery life since the side reactions seldom happen in solid electrolyte systems. Therefore, finding an appropriate solid electrolyte for all-solid state batteries is becoming an important issue.

The NASICON structure, which is referred to the family of $Na_{1+x}Zr_2Si_xP_{3-x}O_{12}$ ($0<x<3$),[14–19] is famous for its high ionic conductivity. The discovery of the NASICON family has made further development in designing the fast Na^+-conductor electrolyte. The 3-D NASICON framework structure enables the material to have good structural stability and fast ion conduction. Hong and Goodenough[20,21] have reported that the ionic conductivity of $Na_{1+x}Zr_2Si_xP_{3-x}O_{12}$ ($0<x<3$) varies according to the stoichiometry of the NASICON composition. The highest conductivity is obtained in the range of $1.8 < x < 2.2$. Especially, the conductivity obtained for the composition $Na_3Zr_2Si_2PO_{12}$ (NZSP) [17,22–24] is comparable to the Na β'' alumina.[21] Recently, the all solid-state battery using $Na_3V_2(PO_4)_3$ (NVP) as electrode and $Na_3Zr_2Si_2PO_{12}$ as electrolyte is attracting attention as a high performance and low cost battery.[25,26] The NASICON-type $Na_3V_2(PO_4)_3$ electrode is becoming a promising

[a] Center for Computational Sciences, University of Tsukuba, 1-1-1 Tennodai, Tsukuba, Ibaraki 305-8577, Japan.
Email: bui.my.gm@u.tsukuba.ac.jp
[b] Graduate School of Pure and Applied Sciences, University of Tsukuba, 1-1-1 Tennodai, Tsukuba, Ibaraki 305-8577, Japan.
sokada@comas.frsc.tsukuba.ac.jp
[c] Global Research Center for Environment and Energy based on Nanomaterials Science (GREEN), Namiki 1-1, Tsukuba, Ibaraki 305-0044, Japan.
[d] Vietnam Japan University, Vietnam National University of Ha noi, 144 Xuan Thuy, Cau Giay, Hanoi, Vietnam
Email: dv.an@vju.ac.vn
[e] Center for Atomic and Molecular Technologies, Graduate School of Engineering, Osaka University. Yamadaoka 2-1, Suita, Osaka 565-0871, Japan.
[f] Computational Materials Science Unit (CMSU), National Institute for Materials Science (NIMS), Sengen 1-2-1, Tsukuba, Ibaraki 305-0047, Japan.
Email: OHNO.Takahisa@nims.go.jp
[g] Institute of Industrial Science, University of Tokyo, Meguro, Tokyo 153-8505, Japan

electrode material by providing better stability and higher ionic conductivity.[27,28] Furthermore, the material can be used as both anode and cathode. Since NVP and NZSP have the same NASICON structure, there is a possibility to study the NVP/NZSP/NVP cell theoretically and experimentally. Since NVP is becoming one of the most promising candidates for cathode material in SIBs, many experiment studies of NVP were made.[29–31] More recently, Bui *et al.*[28] have systematically studied the structure and diffusion mechanism in NVP theoretically. However, to the best of our knowledge, there is still lack of theoretical study of NZSP. Hence, having a thorough understanding of the structural properties and diffusion mechanism in the electrolyte NZSP is becoming more and more necessary.

2. Method

This paper presents the diffusion mechanism of NZSP using the density functional theory (DFT) as implemented in the Vienna ab initio simulation package (VASP).[32] The geometry optimization and electronic structure analysis were carried out with Monkhorst-pack *k*-point sampling of 2×2×2. The wave functions were expanded by plane-wave basis set with a cutoff energy of 500 eV. The generalized gradient approximation (GGA)[33] with PBE functional was used to deal with the exchange and correlation energy. The diffusion study was made by introducing one Na vacancy into the NZSP monoclinic cell of 80 atoms including three formula units (f.u). For the elementary diffusion processes, we defined Na diffusion pathways and then calculated the corresponding activation barriers using the nudged elastic band (NEB)[34] method. The convergence condition of calculated energies and forces were set at 0.01 eV/f.u and 0.01 eV/Å, respectively.

At low temperature, the space group of $Na_{1+x}Zr_2Si_xP_{3-x}O_{12}$ for x < 1.6 and x > 2.4 is rhombohedral $R\bar{3}c$, while that for 1.6 < x <2.4 is monoclinic C2/c. Fig. 1 shows the $Na_3Zr_2Si_2PO_{12}$ structure. $Na_3Zr_2Si_2PO_{12}$ is a three-dimensional framework created by alternative arranged PO_4 and SiO_4 tetrahedral and ZrO_6 octahedral. Each ZrO_6 octahedra shares its corner with six PO_4 or SiO_4 octahedra while each PO_4 or SiO_4 tetrahedra is connected to four ZrO_6 octahedra. This structure creates a "hexagonal bottleneck" whose shortest diameter is 4.6 Å, which is even bigger by twice than the sum of the Na^+ and O^{2-} ionic radii. Such large space enables Na to move through, enhancing the conductivity of the material. There are three different Na sites in the structure: Na_1, Na_2, and Na_3.[21] Each Na_1 site is linked three-dimensionally to two Na_2 sites and four Na_3 sites, while each Na_2 or Na_3 site is connected to two Na_1 sites. The positions of Na_1, Na_2, and Na_3 are shown in Fig. 1. For construction of the material, we considered many Na-vacancy arrangements from the initial structure and then chose the most stable arrangement for further study.

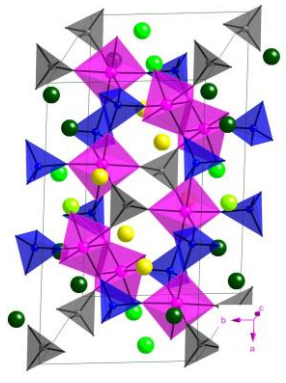

Fig. 1: The crystal structure of $Na_3Zr_2Si_2PO_{12}$. Na at the Na_1 site are shown by yellow balls, Na at the Na_2 site by light green balls, and Na at the Na_3 site by dark green balls. The Zr octahedra are shown by pink, the Si tetrahedra by blue, and the P tetrahedra by grey.

3. Result

Table 1: The experimental and calculated lattice parameters (Å) in $Na_3Zr_2Si_2PO_{12}$.

	a (Å)	b (Å)	c (Å)
Exp.[21]	15.586	9.029	9.205
Calculation	15.801	9.147	9.245

Table 2: The bond distances (Å) of Na_1-O, Na_2-O, Na_3-O P-O, Si-O and Zr-O in $Na_3Zr_2Si_2PO_{12}$.

	Experiment[21]	Calculation
Na_1-O (Å)	2×2.599 2×2.620 2×2.608	2.3636 2.3691 2.3922 2.5270 2.5332 3.0080
Na_2-O (Å)	2×2.413 2×2.600 2×2.808 2×2.974	2×2.4533 2×2.5285 2×2.6181 2×2.7332
Na_3-O (Å)	2.441 2.449 2.478 2.621 2.648 2.772	2.3636 2.3691 2.3922 2.5270 2.5331 3.0081
P-O (Å)	2×1.542 2×1.546	2×1.546 2×1.555
Si-O (Å)	1.543 1.545 1.546 1.583	1.636 1.643 1.643 1.648
Zr-O	2.055 2.077 2.096 2.104 2.137 2.142	1.989 2.060 2.076 2.125 2.146 2.250

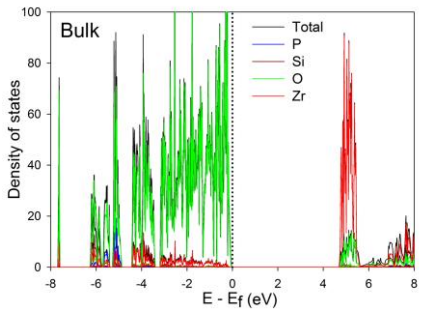

Fig. 2: The density of states for the bulk of $Na_3Zr_2Si_2PO_{12}$

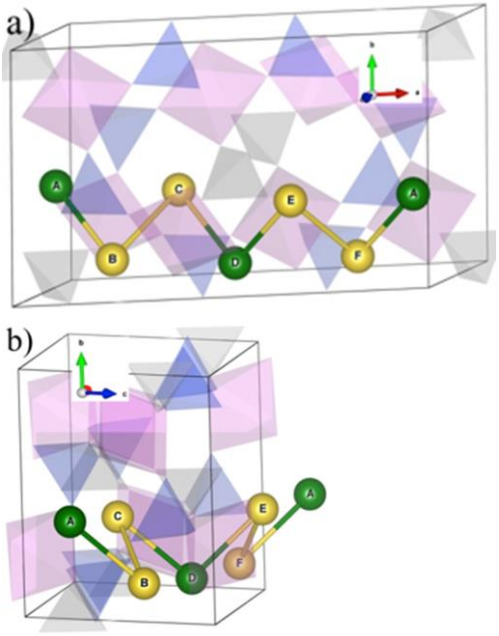

Fig. 3: Schematic of inner-chain processes in Pa. The Na at Na_1 sites are shown in yellow balls while the Na at Na_2 site are shown in green balls. a) c-direction view. b) side view

The obtained structure of $Na_3Zr_2Si_2PO_{12}$ is shown in Fig. 1. The calculated lattice parameters are listed in Table 1. The calculated parameters obtained are a = 15.801 Å, b = 9.147 Å, and c = 9.245 Å. It can be seen that the optimum lattice parameters are in well agreement with the experiment. The bond distances of Na_1-O, Na_2-O, Na_3-O P-O, Si-O and Zr-O are listed in Table 2. We have found that the calculated P-O and Zr-O bond distances are in accordance with the experiment. In the experimental data, the Si-O and P-O bond lengths are almost similar. This is because the structure that the experimentalists proposed was based on the assumption that the Si atoms are ordered in the P positions. Hence, our result of average Si-O bond of 1.643 Å, which is in accordance with other experiments,[23,19] is reasonable. Furthermore, since we realized that the Na_3-O bond length is similar to that of Na_1-O, we can rename Na_3 as Na_1. Hence, in our calculation, there are only two types of Na: Na_1 and Na_2. The formation energy calculations indicate that the vacancy at the Na_2 site is approximately 60 meV lower than that at the Na_1 site.

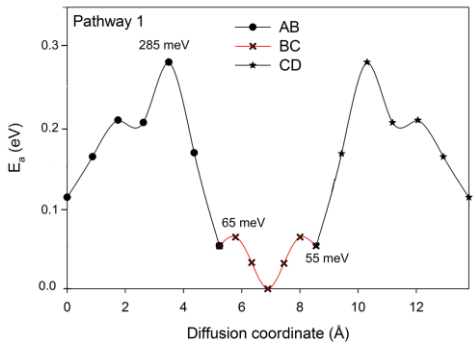

Fig. 4: Activation energies of the Na vacancy diffusion along Processes AB, BC, and CD. The circle, cross, and star symbols represent the activation energy profile of the Processes AB, BC, and CD, respectively.

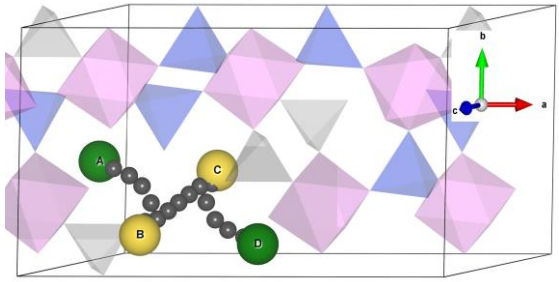

Fig. 5: Diffusion orbit of Processes AB, BC, and CD. Intermediate Na are shown in deep grey balls.

Figure 2 illustrates the non spin-polarized density of state (DOS) of the bulk $Na_3Zr_2Si_2PO_{12}$. The projected DOS on the 3*d*-states of Zr atoms and the 2*p*-states of P, Si, and O atoms are also presented. We found that the valence band is mainly contributed by 2p states of O while the conduction band is dominated by 3d states of Zr. The 3*d*-states of Zr and the 2*p*-states of O are highly localized. Owing to wide band-gap of 4.6 eV, the material can be considered as an insulator.

When a Na vacancy is introduced into the structure, the neighboring Na ions may jump into the vacant site. The Na vacancy sites are indexed as Na_i (i = A, B, C, D, E, and F). Four elementary processes are addressed: three inner-chain processes (Processes AB, BC, and CD) and one inter-chain process (Process BE). The diffusion mechanism in Processes AB, BC, and CD are described as below:

i) Process AB: the Na vacancy diffuses from Na_A to Na_B along $[\bar{2}34]$ direction. The diffusion takes place from the Na_2 to Na_1 site. The diffusion distance is 5.237 Å.

ii) Process BC: the Na vacancy moves from Na_B to Na_C along $[12\bar{1}]$ direction. The diffusion distance is 3.322 Å. Both Na_B and Na_C locate at the Na_1 sites.

iii) Process CD: the Na vacancy jumps from Na_C to Na_D along the direction parallel to the Process AB. The Na vacancy diffuses from the Na_1 site to the Na_2 site with a distance of 5.252 Å.

Note that, the Na diffusion in Processes DE, EF, and FA has the same mechanism as that in Processes AB, BC, and CD, respectively. For more detail:

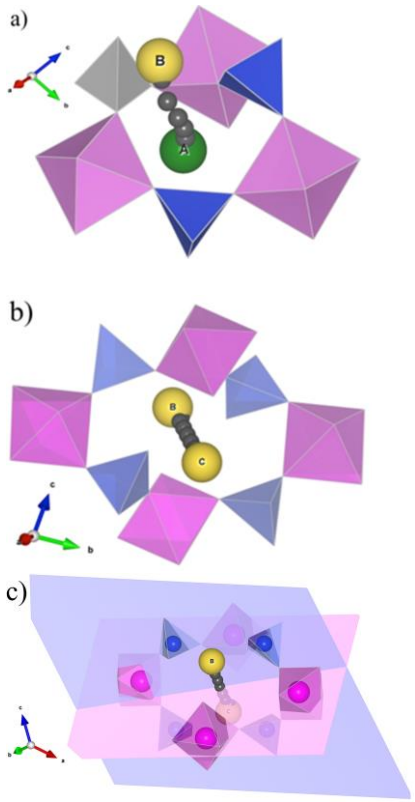

Fig 6: Schematic of Na diffusion through hexagonal bottlenecks and octagonal bottleneck. a) Process AB b) Process BC c) Process BC with planes. The ZrO_6 octahedra and SiO_4 tetrahedra planes are shown in pink and blue, respectively.

iv) Process DE: the Na vacancy moves from Na_D to Na_E along [234] direction. The diffusion distance and activation energy of this process are similar to those of Process AB.

v) Process EF: the Na vacancy migrates from Na_E to Na_F along $[\bar{1}21]$ direction. The diffusion mechanism of this process is similar to that of Process BC.

vi) Process FA: the Na vacancy jumps from Na_F to Na_A along the direction parallel to the process DE. The characteristic of the diffusion in this process is identical to that in Process CD.

The diffusion mechanism in those processes is illustrated in Fig. 3. As seen in Fig. 3b, the diffusion plane of Processes DE, EF, and FA is perpendicular to that of Processes AB, BC, and CD. Figure 4 depicts the activation barrier of inner-chain processes. The energy barrier of Processes AB and CD is 230 meV while that of Process BC is as low as 65 meV. This indicates that, the Na diffusion in Process BC is easier than that in Processes AB and CD. The diffusion trajectory of Processes AB, BC, and CD is depicted in Fig. 5. The Na_A-Na_B (3.7 Å) and Na_B-Na_C (3.9 Å) distances are almost the same. The Na diffusion trajectory of Process BC is straight, while those for Processes AB and CD are parabolic. Therefore, this Na diffusion path in Process BC is shorter than those in Processes AB and CD. In Processes AB and CD, Na migrates through the "hexagonal bottleneck" while Na travels easily through the large "octagonal bottleneck" in Process BC. As seen in Fig. 4, E_a of Process BC is lower than that of Process AB and CD. The images of the diffusion through "hexagonal bottleneck" and "octagonal bottleneck" are shown in Fig. 6. The "octagonal bottleneck" is created by alternatively arranged four ZrO_6 octahedra and four SiO_6 tetrahedra sharing their corner. Four ZrO_6 octahedra lie on $(31\bar{1})$ plane and four SiO_4 tetrahedra stand on (521) plane causing a high symmetry environment as depicted in Fig. 6c. Hence,

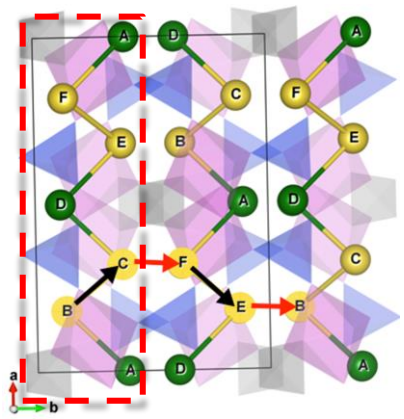

Fig. 7: Schematic of Pb. The Na diffusion chain is indicated by surrounded red dashed line. The black and red arrows indicate the inner-chain processes and inter-chain processes, respectively.

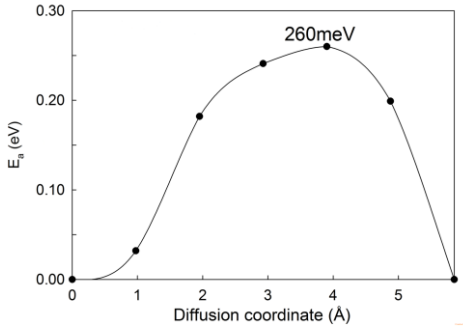

Fig. 8: Activation energies of the Na vacancy diffusion along inter-chain process.

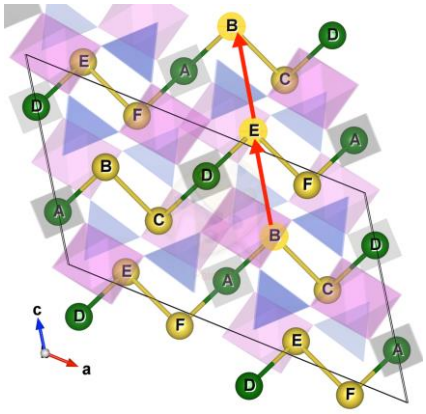

Fig. 9: Schematic of Pc.

when a Na vacancy is introduced at Na_B (Na_C), the Na at Na_C (Na_B) tends to move to the middle point between Na_B and Na_C. The corresponding energy when the Na ion locates at the middle point between B and C sites is 55 meV lower than those of B and C sites as depicted in Fig. 4.

Next, we would like to explain how Na vacancy behaves in inter-chain Process BE. In this process, the Na vacancy diffuses from Na_B to Na_E along [012] direction, with a distance of 5.837 Å. The diffusion happens between Na_1 sites. We have defined the Na diffusion chain, which is indicated by surrounded red dashed line In Fig. 7. Since in Processes AB, BC, CD, DE, EF, and FA, the Na vacancy migrates inside a Na layer, those processes are named as inner-chain processes. In Process BE, Na jumps from one Na diffusion chain to the other chain. Hence, the process is named as an inter-chain process shown by a red arrow in Fig. 7. In this process, Na has to diffuse through the

"hexagonal bottleneck" with activation barrier of 260 meV as depicted in Fig. 8. Note that, the Na diffusion in Process CF has the same mechanism as that in Process BE. In addition, although we also studied other processes such as from Na_B to Na_F, the Na has to climb up a higher energy barrier of 460 meV because there is no "hexagonal bottleneck" or "octagonal bottleneck" appeared along this process.

By combining the possible elementary processes, we can figure out the preferable pathway. In $Na_3Zr_2Si_2PO_{12}$, three preferable pathways are addressed: Pathways a, b, and c. Those pathways are named after their diffusion direction: Pathway a along a direction, Pathway b along b direction, Pathway c along c direction. Pathway a includes inner-chain processes along $Na_A \leftrightarrow Na_B \leftrightarrow Na_C \leftrightarrow Na_D \leftrightarrow Na_E \leftrightarrow Na_F \leftrightarrow Na_A$ path as shown in Fig. 3. The activation energy of 285 meV for the diffusion along this pathway is calculated as the total energy different of the lowest energy inner-chain process BC (E_a = 55 meV) and the highest energy inner-chain process AB (E_a = 230 meV). Pathway b is the combination of inner-chain processes and inter-chain processes along $Na_B \leftrightarrow Na_C \leftrightarrow Na_F \leftrightarrow Na_E \leftrightarrow Na_B$ path as depicted in Fig. 7. The activation barrier for this pathway is calculated to be 315 meV equal to the total energy different of the lowest energy inner-chain process BC (E_a = 55 meV) and the highest energy inter-chain process EB (E_a = 260 meV). Pathway c consists of only inter-chain processes along $Na_B \leftrightarrow Na_E \leftrightarrow Na_B$ path as presented in Fig. 9. The activation barrier for Pathway c is 260 meV. Some authors argued that the dynamic coupling of atom movements to the electronic excited states; i.e. pseudo Jahn-Teller effect, would be a factor to lower the barrier of ion diffusion.[36,37] In the present case, because the energy difference between the $2p^63s^0$ state of Na+ ion and its first excited state $2p^53s^1$ is considerably large, the coupling between these background and excited states hardly occurs. On the other hand, it is clear that the typical structure of the materials includes the wide octahedral and hexahedral bottlenecks. These bottlenecks would help Na ions easily go through, correspondingly, the activation energy of the diffusion would be lower.

4. Conclusion

To sum up, we have investigated the geometrical and the electronic structure, and the Na diffusion mechanism in $Na_3Zr_2Si_2PO_{12}$ based on the density functional theory. The obtained lattice parameters and bond lengths of the structure are in accordance with the experiment. Two Na sites were found: Na_1 and Na_2. In inter-chain processes, Na should move through the "hexagonal bottleneck". In inner-chain processes in which Na moves between the Na_1 site to Na_2 site, Na has to diffuse through the "hexagonal bottleneck". But in inner-chain processes in which Na moves between the same Na_1 sites, Na moves easily across the "octagonal bottleneck". The three dimensional diffusion is confirmed in this study. Pathways Pa, Pb, and Pc that consist of inner-chain and inter-chain processes are examined. The activation barriers for Pathways Pa, Pb, and Pc are 285 meV, 315 meV, and 260 meV, respectively. The material exhibits high ionic conductivity with three-dimensional diffusion.

Acknowledgments:

This work was supported by the MEXT Program for Development of Environment Technology using Nanotechnology. K.M.Bui is grateful to Dr. M. Khazaei for the valuable discussion.

Notes and references

1 J.-M. Tarascon, *Nat. Chem.*, 2010, **2**, 510–510.
2 J. B. Goodenough and Y. Kim, *Chem. Mater.*, 2010, **22**, 587–603.
3 V. A. Dinh, J. Nara and T. Ohno, *Appl. Phys. Express*, 2012, **5**, 045801.
4 K. M. Bui, V. A. Dinh and T. Ohno, *J. Phys. Conf. Ser.*, 2013, **454**, 012061.
5 K. M. Bui, V. A. Dinh and T. Ohno, *Appl. Phys. Express*, 2012, **5**, 125802.
6 D. M. Duong, V. A. Dinh and T. Ohno, *Appl. Phys. Express*, 2013, **6**, 115801.
7 *Practical Handbook of Physical Properties of Rocks & Minerals*, CRC Press, Boca Raton, Fla, 1 edition., 1988.
8 N. Yabuuchi, K. Kubota, M. Dahbi and S. Komaba, *Chem. Rev.*, 2014, **114**, 11636–11682.
9 V. Palomares, P. Serras, I. Villaluenga, K. B. Hueso, J. Carretero-González and T. Rojo, *Energy Environ. Sci.*, 2012, **5**, 5884–5901.
10 B. L. Ellis and L. F. Nazar, *Curr. Opin. Solid State Mater. Sci.*, 2012, **16**, 168–177.
11 M. D. Slater, D. Kim, E. Lee and C. S. Johnson, *Adv. Funct. Mater.*, 2013, **23**, 947–958.
12 J.-M. Tarascon and M. Armand, *Nature*, 2001, **414**, 359–367.
13 K. Takada, *Acta Mater.*, 2013, **61**, 759–770.
14 R. M. Hazen, L. W. Finger, D. K. Agrawal, H. A. McKinstry and A. J. Perrotta, *J. Mater. Res.*, 1987, **2**, 329–337.
15 J. P. Boilot, G. Collin and P. Colomban, *Mater. Res. Bull.*, 1987, **22**, 669–676.
16 J. P. Boilot, G. Collin and P. Colomban, *J. Solid State Chem.*, 1988, **73**, 160–171.
17 O. Bohnke, S. Ronchetti and D. Mazza, *Solid State Ion.*, 1999, **122**, 127–136.
18 U. Warhus, J. Maier and A. Rabenau, *J. Solid State Chem.*, 1988, **72**, 113–125.
19 D. T. Qui, J. J. Capponi, J. C. Joubert and R. D. Shannon, *J. Solid State Chem. Fr.*, 1981, **39**, 219–229.
20 J. B. Goodenough, H. Y.-P. Hong and J. A. Kafalas, *Mater. Res. Bull.*, 1976, **11**, 203–220.
21 H.-P. Hong, *Mater. Res. Bull.*, 1976, **11**, 173–182.
22 N. G. Bukun, *Ionics*, 1996, **2**, 63–68.
23 P. P. Kumar and S. Yashonath, *J. Phys. Chem. B*, 2002, **106**, 7081–7089.
24 M. L. Di Vona, E. Traversa and S. Licoccia, *Chem. Mater.*, 2001, **13**, 141–144.
25 F. Lalère, J. B. Leriche, M. Courty, S. Boulineau, V. Viallet, C. Masquelier and V. Seznec, *J. Power Sources*, 2014, **247**, 975–980.
26 Y. Noguchi, E. Kobayashi, L. S. Plashnitsa, S. Okada and J. Yamaki, *Electrochimica Acta*, 2013, **101**, 59–65.
27 S. Y. Lim, H. Kim, R. A. Shakoor, Y. Jung and J. W. Choi, *J. Electrochem. Soc.*, 2012, **159**, A1393–A1397.
28 K. M. Bui, V. A. Dinh, S. Okada and T. Ohno, *Phys Chem Chem Phys*, 2015, **17**, 30433–30439.
29 W. Song, X. Ji, Z. Wu, Y. Zhu, F. Li, Y. Yao and C. E. Banks, *RSC Adv.*, 2014, **4**, 11375–11383.
30 K. Saravanan, C. W. Mason, A. Rudola, K. H. Wong and P. Balaya, *Adv. Energy Mater.*, 2013, **3**, 444–450.
31 Y. Uebou, T. Kiyabu, S. Okada and J. Yamaki, *Rep. Inst. Adv. Mater. Study Kyushu Univ.*, 2002, **16**, 1–5.
32 G. Kresse and J. Hafner, *Phys. Rev. B*, 1993, **47**, 558–561.
33 J. P. Perdew, K. Burke and M. Ernzerhof, *Phys. Rev. Lett.*, 1996, **77**, 3865–3868.

34 G. Henkelman and H. Jónsson, *J. Chem. Phys.*, 2000, **113**, 9978–9985.
35 S.-M. Lee, S.-T. Lee, D.-H. Lee, S.-H. Lee, S.-S. Han and S.-K. Lim, *J. Ceram. Process Res.*, 2015, **16**, 49.
36 Y. Kamon, H. Harima, A. Yanase and H. Katayama-Yoshida, *Physica B,* 2001, **308–310**, 391–395.
37 K. Shirai, T. Michikita and H. Katayama-Yoshida, *Jpn. J. Appl. Phys.* 2005, **44**, 7760-7764.

